Journal of Alloys and Compounds 509 (2011) 9038–9044

Contents lists available at ScienceDirect

Journal of Alloys and Compounds

journal homepage: www.elsevier.com/locate/jallcom

Influence of titanium addition on the microstructure of the novel ferrous-based stainless steel

Chia-Cheng Lin[a,b], Li-Hsiang Lin[b,c,d], Jing-Ming Hung[b,c,d], Yung-Hsun Shih[b,d,e], Ching-Zong Wu[b,c,d], Keng-Liang Ou[b,f,g,**], Chih-Yeh Chao[h,*]

[a] Shin Kong Wu-Ho-Su Memorial Hospital, Taipei 110, Taiwan
[b] Research Center for Biomedical Devices, Taipei Medical University, Taipei 110, Taiwan
[c] Department of Dentistry, Taipei Medical University Hospital, Taipei 110, Taiwan
[d] School of Dentistry, College of Oral Medicine, Taipei Medical University, Taipei 110, Taiwan
[e] Dental Department of Wan-Fang Hospital, Taipei Medical University, Taipei 110, Taiwan
[f] Research Center for Biomedical Implants and Microsurgery Devices, Taipei Medical University, Taipei 110, Taiwan
[g] Graduate Institute of Biomedical Materials and Engineering, Taipei Medical University, Taipei 110, Taiwan
[h] Department of Mechanical Engineering, Pingtung University of Science and Technology, PingTung 912, Taiwan

ARTICLE INFO

Article history:
Received 14 December 2010
Received in revised form 22 February 2011
Accepted 30 March 2011
Available online 7 April 2011

Keywords:
Fe–Al–Mn–C–Ti alloy
TiC_x carbide
Microstructure
Phase transformation

ABSTRACT

The microstructural characteristics of the Fe–9Al–30Mn–1C–5Ti (wt.%) alloy were determined by scanning electron microscopy, transmission electron microscopy, and energy-dispersive X-ray spectrometry. The microstructure of the alloy was essentially a mixture of $(\gamma + TiC_x + (\alpha + B2 + DO_3))$ phases during solution treatment between 950 °C and 1150 °C. The TiC_x carbide had a face-center-cubic structure with a lattice parameter a of 0.432 nm. When the as-quenched alloy was subjected to aging treatment at temperatures of 450–850 °C, the following microstructural transformation occurred: $(\gamma + TiC_x + \kappa + (\alpha + DO_3)) \rightarrow (\gamma + TiC_x + \kappa + (\alpha + B2 + DO_3 + TiC_x)) \rightarrow (\gamma + TiC_x + \kappa + \kappa' + (\alpha + B2 + DO_3)) \rightarrow (\gamma + TiC_x + (\alpha + B2 + DO_3))$. Addition of Ti promotes the formation of the α phase at high temperatures.

1. Introduction

Austenitic stainless steels have been developed as potential materials for biomedical applications such as dental implants, bone plates, crowns, artificial vascular stents, and screws for fracture fixation owing to their excellent combination of nonmagnetic properties, strength, ductility, workability, corrosion resistance, and excellent biocompatibility [1–3]. However, conventional Fe–Cr–Ni-based stainless steels contain expensive alloying elements (Ni and Cr). Thus, from an economic point of view, it is desirable to substitute Ni and Cr with cheaper elements while maintaining the desirable mechanical and biological properties outlined above.

Fe–Al–Mn ternary alloy system is a promising alternative to some conventional Fe–Cr–Ni-based stainless steels, because it substitutes Cr and Ni with the lighter and cheaper elements Al and Mn [4,5]. In Fe–Al–Mn alloy, Al stabilizes the ferritic phase and improves anti-corrosion behavior by forming a continuous protective Al_2O_3 layer on the surface [4–6]. The addition of Mn serves to stabilize the austenitic structure and also enhances mechanical properties at high temperatures [5,7,8]. Carbon plays an important role in promoting the precipitation strength of Fe–Al–Mn alloy, which is necessary for high strength [8,9]. Chang et al. [10] reported that the optimal aging temperature was 450 °C, which resulted in the Fe–Al–Mn–C alloy possessing high yield strength of 1383 MPa with 32.5% elongation.

Moreover, other metallic elements such as Si, Cu, Ti, V, Co, and Cr may be added in order to increase the corrosion and oxidation resistance as well as improve strength [5,11–16]. Our previous studies showed that some carbides were formed on Fe–Al–Mn and Fe–Al–Mn–C-based alloys following phase transformation by heat-treatment and surface functionalization [16,17]. These carbides play an important role in the formation of nanostructures and oxidation layers, and they also help increase biocompatibility. Therefore, the Fe–Al–Mn–C-base alloys not only possess excellent mechanical properties but also exhibit good biocompatibility, which make them potential candidates for biomedical applications. As stated above, the purpose of the present study is to

* Corresponding author. Tel.: +886 8 7703202x7116.
** Co-corresponding author at: Graduate Institute of Biomedical Materials and Engineering, Taipei Medical University, Taipei 110, Taiwan.
Tel.: +886 2 27361661x5400.
E-mail addresses: klou@tmu.edu.tw (K.-L. Ou), cychao@mail.npust.edu.tw (C.-Y. Chao).

0925-8388/$ – see front matter © 2011 Elsevier B.V. All rights reserved.
doi:10.1016/j.jallcom.2011.03.174

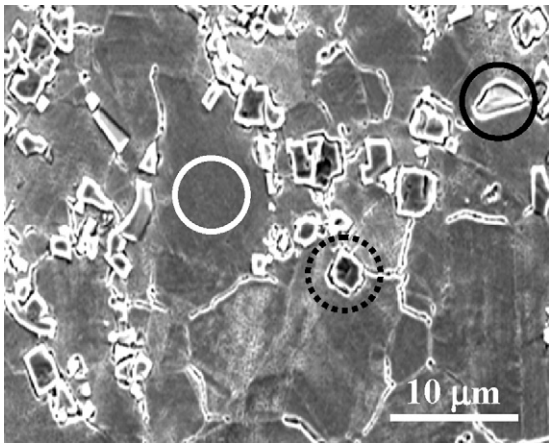

Fig. 1. SEM image of the present alloy underwent solution treatment at 950 °C for 1 h.

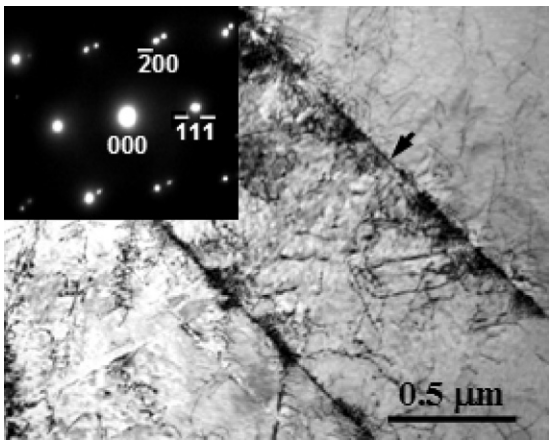

Fig. 2. A zone axis [0 1 1] BF image taken from the matrix, which is marked as white circle in Fig. 1.

investigate the effect of adding 5 wt.% Ti on the microstructure of Fe–9Al–30Mn–1C alloy and thus to provide information relevant for biomedical applications.

2. Experimental procedures

Fe–9Al–30Mn–1C alloy containing 5.0 wt.% Ti was prepared in an air induction furnace under a protective N_2 atmosphere using AISI 1008 low carbon steel, 99.7% pure electrolytic Al, 99.9% pure electrolytic Mn, pure C powder, and pure Ti. The alloy was poured into an investment casting steel mould (ϕ 40 mm × 100 mm) that had been preheated to 1100 °C. The chemical composition of the investigated alloy, as determined by inductively coupled plasma atomic emission spectrometry, was Fe–8.82Al–30.15Mn–0.94C–4.93Ti (wt.%). The ingots were hot-forged to a final thickness of 3.0 mm following homogenization at 1200 °C for 4 h under a protective argon atmosphere. The as-forged specimens were subsequently heat-treated at temperatures ranging from 450 °C to 1150 °C for various periods in a vacuum furnace and then rapidly water quenched. Specimens for scanning electron microscopy (SEM; JEOL JSM-6500F) were abraded with SiC paper, polished with 0.3 μm Al_2O_3 powder, washed in distilled water, ultrasonically degreased in acetone, and etched with 5–10% nital solution. Transmission electron microscopy

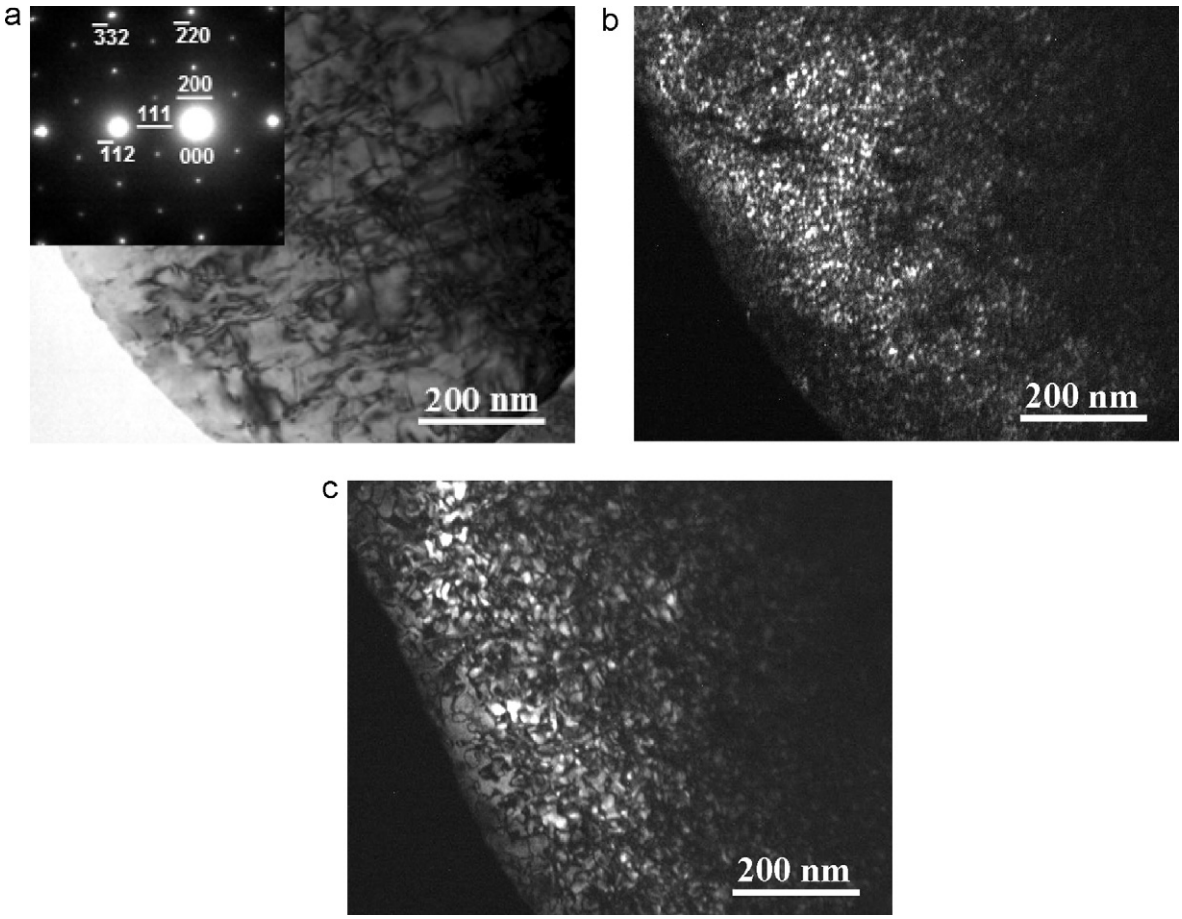

Fig. 3. (a) a zone axis [1 1 0] BF image taken from the island-like phase, which is marked as black circle in Fig. 1 ($h\,k\,l$ = α phase, $h\,k\,l$ = DO_3 phase), (b) and (c) are two $\vec{g} = 1\ \ 1\ \ 1$ and $\vec{g} = 2\ \ 0\ \ 0$ DF images, respectively.

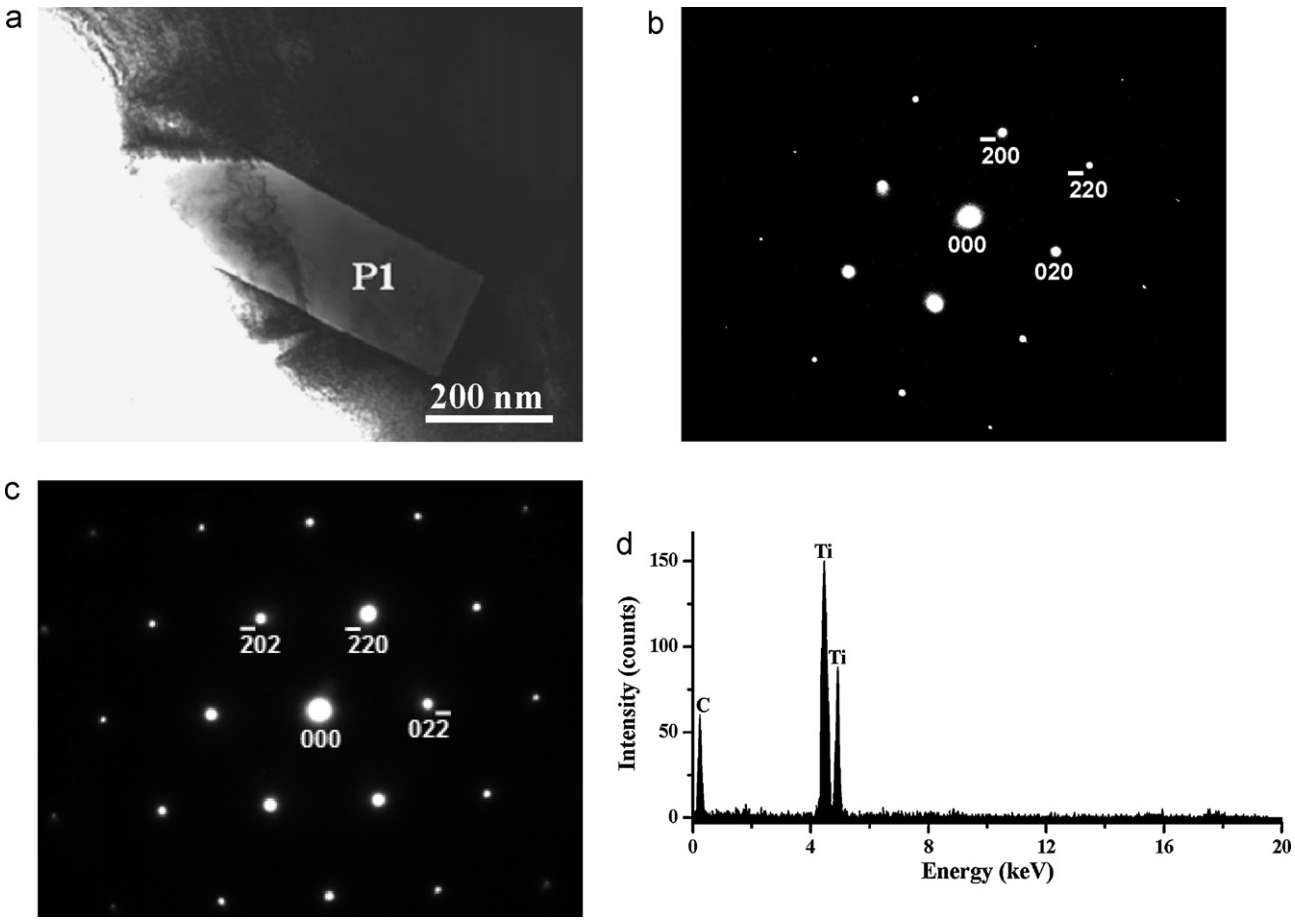

Fig. 4. (a) a BF image taken from the square-like phase, which is marked as black dashed line circle in Fig. 1, (b) and (c) are two SAEDPs taken along [0 0 1] and [1 1 1] from the P1 phase, respectively, (d) chemical compositions of the P1 phase.

(TEM) was conducted using a JEOL-2100 operated at 200 kV. Elemental distributions were examined using an INCA energy-dispersive X-ray spectrometer (EDS). The average atomic percentages of alloying elements were determined by analyzing at least ten different EDS spectra for each phase. Thin foils for TEM were prepared by mechanical grinding down to 30 μm thickness and subsequent electropolishing using an electrolyte containing 60% ethanol, 30% acetic acid, and 10% perchloric acid at a current density of 1.5–2.5 × 10^4 A/m^2 at temperatures less than −10 °C.

3. Results and discussion

Fig. 1 shows an SEM image of the alloy after solution treatment at 950 °C for 1 h; the presence of precipitates in the matrix and at grain boundaries is clearly evident. It was found that the microstructure of the alloy could be divided into an island-like phase, a square-like phase, and the matrix regions (denoted by black circle, black dashed line circle, and white circle, respectively). These microstructural characteristics are similar to that of the as-quenched Fe–Al–Mn–C–Cr alloy [14]. The alloy was further analyzed by TEM. Fig. 2 shows a zone axis [0 1 1] bright-field (BF) image taken from the matrix [white circle in Fig. 1], revealing the matrix is the austenite phase (γ) with a face-center-cubic (FCC) structure and a lattice parameter *a* of 0.380 nm. Furthermore, some dislocations and annealing twins (as indicated by the arrow) with a (1 1 1) habit plane can be observed within the γ matrix [14,18]. No other precipitates could be detected within the γ matrix.

Fig. 3(a) displays a zone axis [1 1 0] BF image taken from the island-like phase [black circle in Fig. 1]. Obviously, a high density of dislocations exists within the island-like phase. The selected area electron diffraction pattern (SAEDP) contained not just the reflection spots of the ferrite (α) phase [*h k l*] with body-center-cubic (BCC) structure but also other superlattice spots [*h k l*]. It has been suggested that these superlattice spots are the DO_3 ($(Fe,Mn)_3Al$) phase with a F_{m3m} structure [19] and lattice parameter *a* of 0.565 nm. Nevertheless, it was also found that the $\vec{g} = 2\ 0\ 0$ reflection intensity is much stronger than the $\vec{g} = 1\ 1\ 1$ reflection intensity in the DO_3 phase. This demonstrates that the DO_3 phase and the B2 ((Fe,Mn)Al) phase with CsCl structure [19] and lattice parameter *a* of 0.282 nm may coexist in the same $\vec{g} = 2\ 0\ 0$ reflection spot. If such a situation has occurred, the B2 phase shown in the dark-field (DF) image of 2 0 0 DO_3 reflections would be expected to be larger than the DO_3 phase as shown in the 1 1 1 DO_3 reflections for the continuous ordering transition [4,14,20]. Fig. 3(b) and (c) are two $\vec{g} = 1\ 1\ 1$ and $\vec{g} = 2\ 0\ 0$ DO_3 phase DF images, respectively. It is clear that the 2 0 0 DO_3 (Fig. 3(c)) is larger than the 1 1 1 DO_3, as shown in Fig. 3(b). Thus, we have conclusively demonstrated that the B2 phase is also formed within the α phase in this study. This result is in agreement with observations reported by other researchers for Fe–Al–Mn–C [4] and Fe–Al–Mn–C–Cr alloys [14]. As a result, the microstructure of the island-like phase is a mixture of (α + B2 + DO_3) phases.

Fig. 4(a) shows a BF image taken from a square-like phase [black dashed line circle, Fig. 1]. A square-like phase (denoted as P1) is formed in the matrix. Figs. 4(b) and (c) are two SAEDPs taken along [0 0 1] and [1 1 1] from the P1 phase, respectively. On the basis of the camera length and *d*-spacings of the spots, it can be concluded that the P1 phase possesses a FCC structure with a lattice parameter *a* of 0.432 nm. Fig. 4(d) presents the chemical compositions of the P1 phase, revealing that the phase is TiC_x carbide [21]. Hence, the

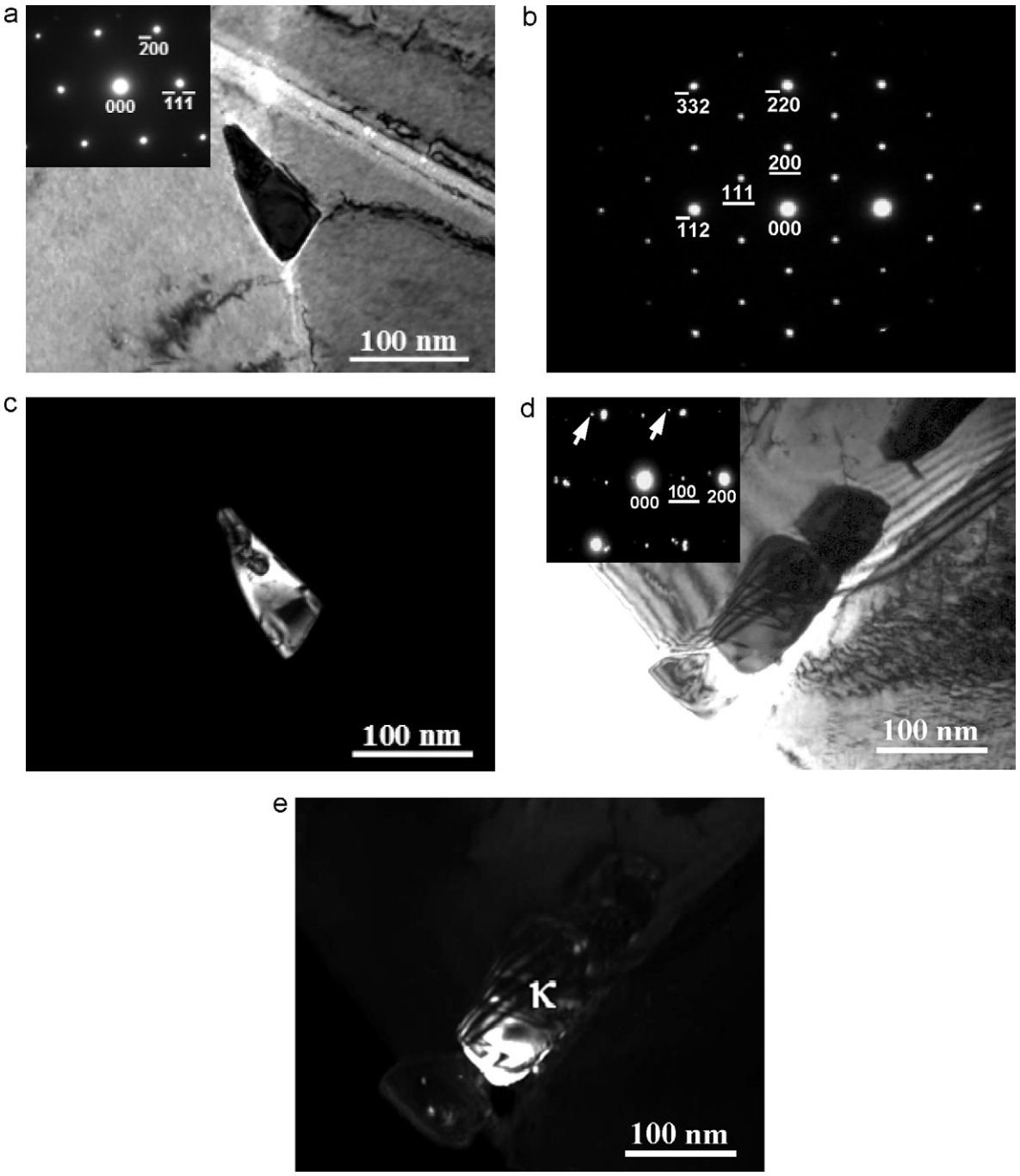

Fig. 5. (a) a zone axis [0 1 1] BF image taken from the γ/γ boundary of the as-quenched alloy aged at 450 °C for 24 h, (b) a SAEDP taken along [0 1 1] from the triangle-like phase in (a), (c) a $\vec{g} = 2\ 0\ 0$ DO_3 DF image, (d) a zone axis [0 1 $\bar{1}$] BF image taken from the γ/α boundary of the alloy (*h k l* = γ phase, *h k l* = κ-phase) and (e) a $\vec{g} = 1\ 0\ 0$ κ-phase DF image.

microstructure of the alloy after solution treatment at 950 °C for 1 h suggests that it comprises the (γ + TiC_x + (α + B2 + DO_3)) phase. As the temperature increases to between 1050 °C and 1150 °C, no significant differences in the microstructure were observed when compared with Fig. 1.

After quenching at 1150 °C for 1 h, the specimens were subsequently aged at temperatures ranging from 450 °C to 850 °C for moderate times. The microstructural properties of the as-quenched alloy aged at 450 °C for 8 h was essentially the same as that seen in Fig. 1. However, after aging for 24 h, a microstructural transition could be seen in the matrix and at the grain boundaries of the alloy. Fig. 5(a) displays a zone axis [0 1 1] BF image taken from the γ/γ boundary of the as-quenched alloy aged at 450 °C for 24 h, which clearly shows the presence of a triangle-like phase at the γ/γ boundary. Fig. 5(b) is an SAEDP taken along [0 1 1] from the triangle-like phase in Fig. 5(a), indicating that the triangle-like phase is also an α phase belonging to a BCC structure. Moreover, it is noteworthy to mention that only the DO_3 (F_{m3m}) phase consists of an α phase because the $\vec{g} = 2\ 0\ 0$ reflection intensity is similar to the $\vec{g} = 1\ 1\ 1$ reflection intensity [14,20]. Fig. 5(c) illustrates a DF image taken from $\vec{g} = 2\ 0\ 0$ DO_3 phase. Thus, the microstructure of triangle-like phase comprises α and DO_3 phases. Furthermore, particulate precipitate was also found at the grain boundary. Fig. 5(d) is a zone axis [0 1 $\bar{1}$] BF image taken from the

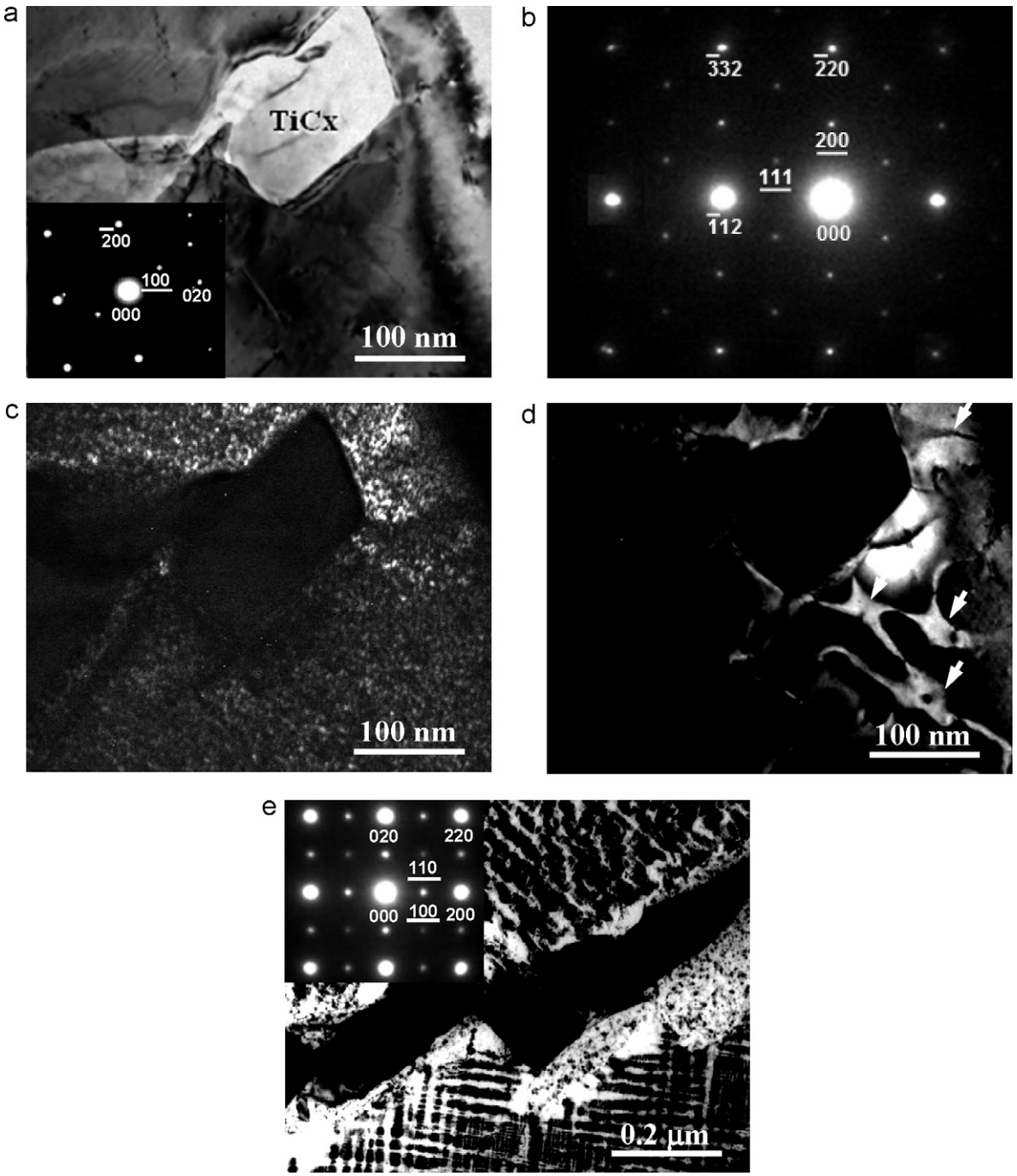

Fig. 6. (a) a zone axis [0 0 1] BF image taken from the α domain of the as-quenched alloy aged at 550 °C for 24 h, (b) a zone axis [1 1 0] SAEDP taken from the α domain in (a), (c) and (d) are two $\vec{g} = 1\ \ 1\ \ 1$ and $\vec{g} = 2\ \ 0\ \ 0$ DO_3 phase DF images, respectively, (e) a BF image taken along [0 0 1] from the γ/γ boundary of the alloy (hkl = γ phase, hkl = κ-phase).

γ/α boundary of as-quenched alloy aged at 450 °C for 24 h, revealing that in addition to the reflection spots of the α phase (indicated by the arrows) and γ phase, the SAEDP also comprises small superlattice spots. From the camera length and *d*-spacings of the spots, the particle is identified as κ-phase carbide ($(Fe,Mn)_3AlC_x$) having an order $L'1_2$ structure [9,15] with a lattice parameter *a* of 0.385 nm. Fig. 5(e) presents a $\vec{g} = 1\ \ 0\ \ 0$ κ-phase DF image, clearly showing the presence of the κ-phase at the γ/α boundary. Furthermore, the TiC_x carbide can also be observed in the matrix and at grain boundaries. Thus, we can state that the microstructure of the as-quenched alloy aged at 450 °C for 24 h is the (γ + TiC_x + κ + (α + DO_3)) phase.

After the aging temperature was increased to 550 °C for a period less than 16 h, it was found that the phase relationships and microstructure features of the alloy were identical to the alloy aged at 450 °C for 24 h (i.e. Fig. 5). When the soaking time was increased to 24 h, TiC_x carbide formed in the α (BCC) domain, as shown in Fig. 6(a). Fig. 6(b) displays a zone axis [0 1 1] SAEDP taken from the α domain in Fig. 6(a). From the $\vec{g} = 1\ \ 1\ \ 1$ and $\vec{g} = 2\ \ 0\ \ 0$ reflection intensity, it can be proven that the B2 (CsCl) and DO_3 (F_{m3m}) phases coexist within the α domain [20]. Fig. 6(c) and 6(d) are two $\vec{g} = 1\ \ 1\ \ 1$ and $\vec{g} = 2\ \ 0\ \ 0$ DO_3 phase DF images, respectively. Fine DO_3 domains with 1/4 *a*(1 1 1) anti-phase boundaries and coarse B2 domains with 1/4 *a*(2 0 0) anti-phase boundaries

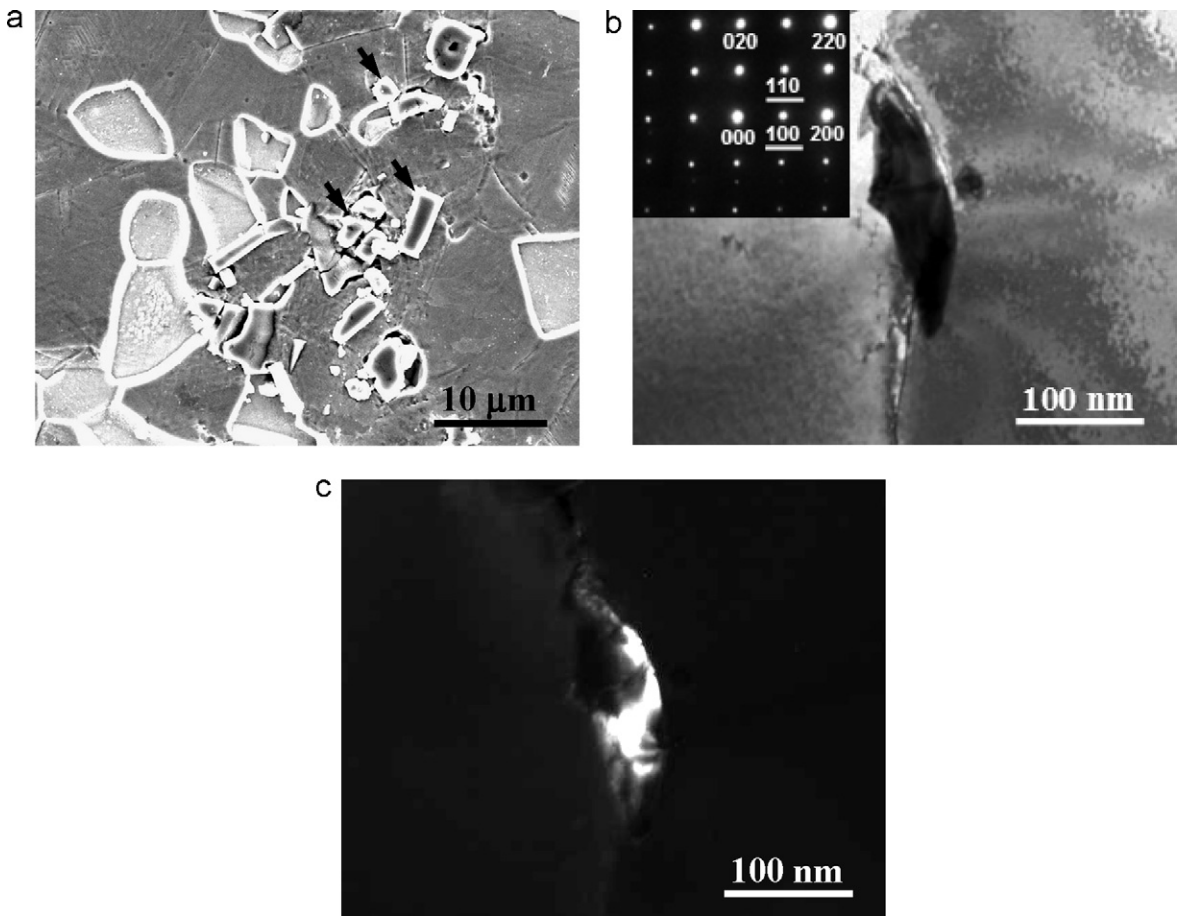

Fig. 7. (a) SEM image of the as-quenched alloy aged at 750 °C for 16 h, (b) a BF image taken along [0 0 1] from the γ/γ boundary of the alloy in (a) (*h k l* = γ phase, *h k l* = κ-phase), and (c) a $\vec{g} = 1\ \ 0\ \ 0$ κ′-phase DF image.

(indicated by the white arrows) can be observed in the α domain [4,14]. Moreover, the κ-phase carbides can also be detected in the matrix and at grain boundaries, as shown in Fig. 6(e). Hence, the microstructure of the as-quenched alloy aged at 550 °C for 24 h is the (γ + TiC_x + κ + (α + B2 + DO_3 + TiC_x)) phase. The TiC_x phase not only formed in the matrix but also precipitated within the α phase.

When the aging temperature was increased to 650 °C for various soaking times, the microstructure characteristics of the alloy was same as Fig. 6. As the alloy underwent aging treatment at 750 °C for a periods longer than 16 h, the TiC_x phase could not be detected within the α phase and the amounts of TiC_x phase (as indicated by the arrows) significantly decreased as depicted in Fig. 7(a). Nevertheless, it was found that some particles start to appear at the grain boundaries. A BF image taken along [0 0 1] from the γ/γ boundary of the alloy (Fig. 7(b)) clearly shows the formation of particles at the grain boundary. Moreover, in addition to the reflection spots of the γ phase, the SAEDP also comprises small superlattice spots. From the camera length and *d*-spacings of the spots, the particle also belongs to κ-phase carbide. However, Chao et al. [9] demonstrated that the intensity of the (1 0 0) spot for the $L'1_2$ structure is much stronger than that of the (1 1 0) spot. Furthermore, the intensities of the (1 0 0) and (1 1 0) spots of the $L1_2$ structure are similar. Therefore, it was concluded that the particles correspond to κ′-phase carbide ($(Fe,Mn)_3AlC_x$) having an ordered $L1_2$ [22] structure with a lattice constant *a* of 0.387 nm. Fig. 7(c) which shows a $\vec{g} = 1\ \ 0\ \ 0$ κ′-phase DF image, reveals the presence of the κ′-phase at the γ/γ boundary. Therefore, the microstructure of the as-quenched alloy aged at 750 °C for 16 h changes to the (γ + TiC_x + κ + κ′ + (α + B2 + DO_3)) phase. After a prolonged aging at 850 °C, no κ-phase and κ′-phase could be observed in the matrix and at the grain boundaries, but it was found that the amounts of TiC_x phase greatly increased with soaking time. Hence, its macrostructure changed to a mixture of (γ + TiC_x + (α + B2 + DO_3)) phases. In summary, when the as-quenched alloy was aged at temperatures ranging from 450 °C to 850 °C, the following microstructural transformation sequence occurred: (γ + TiC_x + κ + (α + DO_3)) → (γ + TiC_x + κ + (α + B2 + DO_3 + TiC_x)) → (γ + TiCx + κ + κ′ + (α + B2 + DO_3)) → (γ + TiC_x + (α + B2 + DO_3)).

According to the Fe–Al–Mn–C quaternary phase diagram [23], the microstructures of Fe-(6.0–11.0)Al-(20.0–35.0)Mn-(0.5–1.5)C (wt.%) alloys heat treated between 950 °C and 1150 °C are full γ phase. Moreover, as the metallic elements Co and Cr were added into the Fe–Al–Mn–C alloy, and following solution treatment at high temperatures, the microstructure is an essential single γ phase with annealing twins [12,13,15]. However, it was found that when the investigated alloy undergoes a solution treatment at temperatures ranging from 950 to 1150 °C, the microstructure is (α + γ) containing TiC_x carbide. These observations clearly highlight the influence of Ti addition; such an addition promotes the formation of α phase in the Fe–Al–Mn–C alloy at high temperatures. It make be proposed that Ti that has a stronger bonding energy with C [20] than either Co or Cr. Hence, when the alloy undergoes solution treatment at high temperatures, a large number of TiC_x carbide may be formed in the matrix and at the grain boundaries as seen in Fig. 1. Carbon not only strengthens but it also increases the stability of the γ phase [8,9]. Table 1 presents quantitative chemical compositions of the γ phase and TiC_x carbide of the alloy after solution treatment at 1150 °C for 1 h. It is clear that the concentration of C

Table 1
The chemical compositions of the γ phase and TiC_x carbide of the alloy underwent solution treatment at 1150 °C for 1 h.

Solution treatment	Phase	Chemical composition (wt.%)				
		Fe	Al	Mn	C	Ti
1150 °C – 1 h	γ	Bal.	8.42	32.14	0.85	2.74
	TiC_x	Bal.	3.52	5.24	15.42	70.23

in the γ phase is lower than that of the TiC_x carbide. Thus, formation of the TiC_x carbide leads to a marked decrease in carbon in the γ matrix thus causing a $\gamma \rightarrow (\alpha + \gamma)$ transition in the matrix of the alloy. It has been reported that the formation of carbide plays a vital role in forming surface micro-porosity structure and in increasing the thickness of the oxide layer, thus improving the alloy biocompatibility [16]. Therefore, it may be supposed that the presence of TiC_x carbide in the present alloy may also increase the alloy biocompatibility. Finally, it is worthwhile to note that further tests are required to evaluate the biocompatibility, corrosion and mechanical properties of the Fe–Al–Mn–C–Ti alloy prior to use in biomedical applications.

4. Conclusions

The microstructure of the as-quenched alloy is a mixture of the γ, α, and TiC_x phases. Moreover, an $\alpha \rightarrow B2 \rightarrow DO_3$ phase transition sequence could be observed within the α region. At different aging temperatures ranging from 450 °C to 650 °C, κ-phase carbide ($(Fe,Mn)_3AlC_x$) with an ordered $L'1_2$-type structure formed at the α/γ grain boundaries, and the $(\alpha + DO_3)$ phase could be observed at the γ/γ grain boundaries. In addition, the TiC_x carbide precipitated within the α region of the as-quenched alloy aged at 500 °C for 24 h. When the as-quenched alloy was aged at 750 °C, κ′-phase carbides possessing $L1_2$ structure formed at the grain boundaries. Above 850 °C, only the TiC_x carbide could be detected in the matrix. These microstructure features can be useful in further understanding the relationship between the corrosion, mechanical behavior and biocompatibility of the present of alloy, and also in assessing its potential for use as a biomedical material.

Acknowledgements

The authors would like to thank the Center of Excellence for Clinical Trial and Research in Neurology and Neurosurgery, Taipei Medical University-Wan Fang Hospital, for financially supporting this research under contract No. DOH100-TD-B-111-003, supported partly by the Department of Health, Executive Yuan, Taiwan under contract No. DOH100-TD-N-111-004. The authors would also like to thank the Shin Kong Wu Ho-Su Memorial Hospital for financially supporting this research under contract SKH-8302-99-DR-33.

References

[1] G. Mani, M.D. Feldman, D. Patel, C.M. Agrawal, Biomaterials 28 (2007) 1689.
[2] A. Hedayati, A. Najafizadeh, A. Kermanpur, F. Forouzan, J. Mater. Process. Technol. 210 (2010) 1017.
[3] D.F. Williams, Biomaterials 29 (2008) 2941.
[4] W.C. Cheng, C.F. Liu, Y.F. Lai, Mater. Sci. Eng. A 337 (2002) 281.
[5] J.D. Betancur-Rios, K. Nomura, C.J. Wang, G.A. Pérez Alcazar, J.A. Tabares, Hyperfine Interact. 187 (2008) 43.
[6] S.C. Chang, Y.H. Hsiau, M.T. Jahn, J. Mater. Sci. 24 (1989) 1117.
[7] C.J. Wang, Y.C. Chang, Mater. Chem. Phys. 76 (2002) 151.
[8] M.C. Li, H. Chang, P.W. Kao, D. Gan, Mater. Chem. Phys. 59 (1999) 96.
[9] C.Y. Chao, C.H. Liu, Mater. Trans. 43 (2002) 2635.
[10] K.M. Chang, C.G. Chao, T.F. Liu, Scripta Mater. 63 (2010) 162.
[11] B. Bhattacharya, A.S. Sharma, S.S. Hazra, R.K. Ray, Metall. Trans. A 40A (2009) 1190.
[12] C.F. Huang, K.L. Ou, C.S. Chen, C.H. Wang, J. Alloys Compd. 488 (2009) 246.
[13] C.M. Liu, H.C. Cheng, C.Y. Chao, K.L. Ou, J. Alloys Compd. 488 (2009) 52.
[14] M.S. Chen, H.C. Cheng, C.F. Huang, C.Y. Chao, K.L. Ou, C.H. Yu, Mater. Charact. 61 (2010) 206.
[15] C.S. Chen, C.T. Lin, P.W. Peng, M.S. Huang, K.L. Ou, L.H. Lin, C.H. Yu, J. Alloys Compd. 493 (2010) 346.
[16] C.H. Wang, J.W. Luo, C.F. Huang, M.S. Huang, K.L. Ou, C.H. Yu, J. Alloys Compd. 509 (2011) 691.
[17] S.L. Chen, M.H. Lin, C.C. Chen, K.L. Ou, J. Alloys Compd. 456 (2008) 413.
[18] W.C. Cheng, H.Y. Lin, Mater. Sci. Eng. A 341 (2003) 106.
[19] Y.C. Lin, Acta Mater. 18 (1999) 4665.
[20] Y.L. Lin, C.P. Chou, Scripta Metall. 28 (1993) 1261.
[21] N. Frage, L. Levin, E. Manor, R. Shneck, J. Zabicky, Scripta Mater. 35 (1996) 799.
[22] W.K. Choo, J.H. Kim, J.C. Yoon, Acta Mater. 45 (1997) 4877.
[23] K. Ishida, H. Ohtani, N. Satoh, R. Kainuma, T. Nishizawa, ISIJ Int. 30 (8) (1990) 680.